Chinese Chemical Letters 36 (2025) 109728

Contents lists available at ScienceDirect

Chinese Chemical Letters

journal homepage: www.elsevier.com/locate/cclet

# Carbonization-engineered ultrafast chemical reaction on nanointerface

Tiantian Long[a], Hongmei Luo[a], Jingbo Sun[a], Fengniu Lu[b], Yi Chen[c], Dong Xu[a,*], Zhiqin Yuan[d,*]

[a] College of Food Science and Engineering, Central South University of Forestry and Technology, Changsha 410004, China
[b] Department of Chemistry and Chemical Engineering, Beijing Institute of Technology, Beijing 100081, China
[c] Hunan Zhixiangweilai Biotechnology Co., Ltd., Changsha 410125, China
[d] State Key Laboratory of Chemical Resource Engineering, College of Chemistry, Beijing University of Chemical Technology, Beijing 100029, China

ARTICLE INFO

*Article history:*
Received 21 December 2023
Revised 2 February 2024
Accepted 29 February 2024
Available online 6 March 2024

*Keywords:*
Ultrafast reaction kinetics
Carbonization
Electrolysis
Dual-channel response
Multifunctional nanoparticles

ABSTRACT

Ultrafast reaction kinetics is essential for rapid detection, synthesis, and process monitoring, but the intrinsic energy barrier as a basic material property is challenging to tailor. With the involvement of nanointerfacial chemistry, we propose a carbonization-based strategy for achieving ultrafast chemical reaction. In a case study, ultrafast Griess reaction within 1 min through the carbonization of *N*-(1-naphthalene)ethylenediamine (NETH) was realized. The carbonization-mediated ultrafast reaction is attributed to the synergic action of reduced electrostatic repulsion, enriched reactant concentration, and boosted NETH nucleophilicity. The enhanced reaction kinetics in *o*-phenylenediamine-$Cu^{2+}$ and *o*-phenylenediamine-ascorbic acid systems validate the universality of carbonization-engineered ultrafast chemical reaction strategy. The finding of this work offers a novel and simple tactic for the fabrication of multifunctional nanoparticles as ultrafast and effective nanoreactants and/or reporters in analytical, biological, and material aspects.



Chemical reactions with ultrafast kinetics are extremely attractive for diverse aspects, such as steady-state and dynamic sensing, rapid synthesis, and complicated process monitoring [1–7]. The current applications of ultrafast chemical reaction indicate that the intrinsic energy barrier as a basic material property is challenging to tailor. It is recommended that the interfacial reaction possesses fast kinetics due to the altered electric field effect and electron transport, which diminish the reaction energy barrier [8]. Typically, many chemical and photochemical reactions can be dramatically accelerated on aqueous interface, usually called as on-water catalysis [9]. Noteworthy that the different aqueous interfaces endow diverse contributions on reaction kinetics, and considerable research effort has been devoted to the development of ultrafast reactions on different interfaces [10]. Therefore, it is essential to pursue feature aqueous interface contributes to designed and universal ultrafast reaction kinetics.

It is generally accepted that interface area decides the reaction site and is proportional to the reaction kinetics [11,12]. Unfortunately, the construction of large interface area with limited materials is difficult because of the mutually independent phases. A possible solution toward this issue is to form colloidal solution, which provides complete immersion of all interfaces [13]. Recently, carbon nanodots (CDs) synthesized from the carbonization of organic molecules attracts growing attention in various fields due to its strong fluorescence and rich surface reactive residues [14–18]. In consideration of the high specific area, nanoparticles may act as good candidates for realizing ultrafast nanointerfacial reaction. Hence, it is possible to exploit ultrafast chemical reactions on CD surface with effective utilization of the full nanointerface through carbonization strategy.

In this work, we proposed a nanointerfacial chemistry strategy to distinctly accelerate the chemical reaction kinetics based on carbonization. The electrolysis of raw material produced fluorescent CDs and led to the surface attachment of reactive residues with high localized and spatial concentration and enhanced reactivity. Additionally, the formed hydrophilic oxygen-contained group endowed charming nanointerface and facilitated reactant approaching. The synergic action of these factors endows the largely enhanced kinetics of chemical reaction. As a case study, the kinetics of *N*-(1-naphthalene)ethylenediamine (NETH)-involved Griess reaction became ultrafast (within 1 min) on formed NETH-CD surface, which is 15-fold faster than that in typical solution (Fig. 1). The Griess reaction induced rapid responses in both fluorometric and colorimetric variation. The dramatically boosted reaction

* Corresponding authors.
*E-mail addresses:* philip198349@gmail.com (D. Xu), yuanzq@mail.buct.edu.cn (Z. Yuan).

https://doi.org/10.1016/j.cclet.2024.109728
1001-8417/

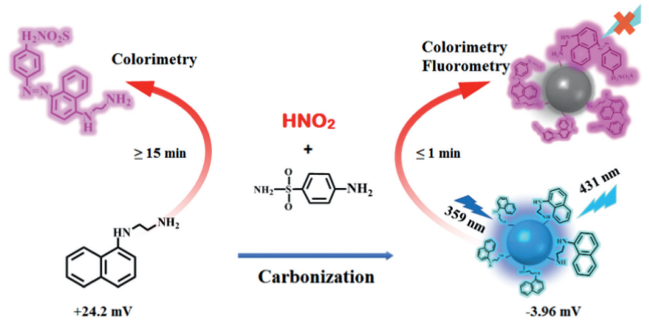


**Fig. 1.** Schematic representation for the carbonization-engineered ultrafast Griess reaction on nanointerface.

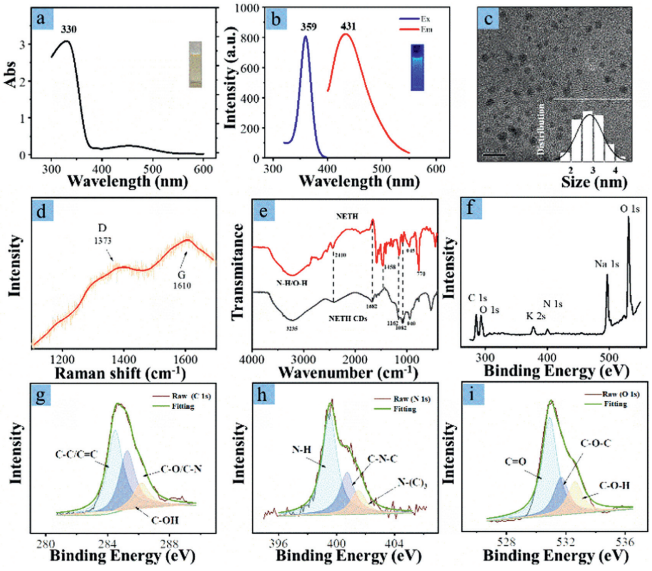


**Fig. 2.** Characterization of NETH-CDs: (a) UV–vis absorption spectra, (b) fluorescence spectra, (c) HRTEM, (d) Raman, (e) FT-IR, and (f) XPS spectra. Inset of (c) The statistical size distribution from HRTEM result. (g-i) Fitted C 1s, N 1s and O 1s XPS spectrum.

kinetics in *o*-phenylenediamine (OPD)-involved ascorbic acid (AA) and $Cu^{2+}$ reaction systems powerfully validated the universality of carbonization-engineered ultrafast chemical reaction strategy. The discovery that nanointerfacial chemistry markedly enhances the reaction kinetics provides valuable guidance for the manufacture of multifunctional nanomaterials towards analytical, biological, and industrial performances.

At the starting point, the synthesis of NETH-CDs was performed through the electrolysis of 0.2 mol/L phosphate buffer (pH 7.4) diluted NETH solution at a voltage of 10 V based on previous reports with modifications [19]. After 15 min electrolysis reaction, the solution showed dark yellow color and emitted blue fluorescence under UV irradiation, indicating the formation of new species (inset in Figs. 2a and b). The as-resulted solution was characterized with UV–vis absorption spectrometry, steady-state and time-resolved fluorescence spectrometry, HRTEM, and XPS. As shown in Fig. 2a, a strong absorption peak around 330 nm and a weak absorption peak around 431 nm were observed. The former is generally assigned to the characteristic absorption of NETH, while the latter is attributed to the formation of NETH-CDs. Through fluorescence measurements, a fluorescent species with maxima excitation and emission wavelengths of 359 and 431 nm appeared (Fig. 2b), suggesting the possible production of NETH-CDs. The absolute fluorescence quantum yield of NETH-CDs was determined to be 4.7%. As manifested in Fig. 2c, the HRTEM image revealed that the as-synthesized NETH-CDs possess quasi-spherical morphology with average diameter of 2.59 nm. The Raman spectra (Fig. 2d) showed two bands centered at 1373 $cm^{-1}$ and 1610 $cm^{-1}$, which belong to D band and G band, respectively. As referred in previous reports, the D band represents the vibration of the defective $sp^2$ carbon region, while the G band represents the vibration of the intact $sp^2$ carbon region [20]. In this case, the intensity ratio of D band and G band ($I_D/I_G$) can be used to describe the content of graphitized carbon in carbon nanomaterials. The $I_D/I_G$ was calculated to be 0.95 (<1), indicating the existence of high graphitization content and low defective carbon structure.

To understand the surface composition, FT-IR spectra of both NETH and NETH-CDs were measured. As shown in Fig. 2e, wide absorption peak around 3200–3350 $cm^{-1}$ belongs to the stretch vibration of N–H was observed in both NETH and NETH-CDs, implying the preservation of amine group of NETH. The peaks at 2410 $cm^{-1}$ and 1458 $cm^{-1}$ were ascribed to –C=N– and C–O–C, respectively [21]. The peak around 1398 $cm^{-1}$ represented the stretching vibration of C-N, the deformation of N–H and C–H groups, while C-OH is at 1162 $cm^{-1}$. The absorption bands near 974, 685 and 505 $cm^{-1}$ were attributed to the stretching vibrations of C–H of aromatic ring. The peak at 1082 $cm^{-1}$ was ascribed to C–O vibration and C-N group stretching, while C=C vibration at 1682 $cm^{-1}$ was observed [22]. The FT-IR characterizations demonstrated the existence of O–H, N–H, –C=N–, and C–O–C groups on NETH-CDs surface.

The surface functional groups of NETH-CDs were further characterized with XPS analysis. It was seen that the characteristic peaks of C 1s, K 2s, N 1s, Na 1s, and O 1s appeared in XPS spectra (Fig. 2f). The Na and K elements are possibly from PBS electrolyte. The content ratio of C, N, and O elements was determined to be about 6:1:12. These three elements are important to CDs function and optical characters, and were individually analyzed. As shown in Fig. 2g, through Gaussian fitting, the C 1s XPS spectra were divided into three peaks, which located at 284.5, 285.2 and 286.1 eV, respectively. These peaks can be assigned to C–C/C=C, C-OH, and C–O/C–N bonds based on previous reports [23]. Accordingly, the N 1s XPS spectra were classified into peaks located around 399.5, 400.7 and 401.5 eV (Fig. 2h), respectively [24]. They could be attributed to N–H, C–N–C, and N–$(C)_3$. In addition, the O 1s XPS spectra comprised C=O, C–O–C, and C–O–H were identified with 531.6, 532.4, and 533.3 eV peaks (Fig. 2i). Taken together, all results demonstrated the successful preparation of NETH-CDs.

Griess reaction is a nitrite-induced NETH-aniline coupling reaction under acidic condition [25], which has been listed as an International Standard (ISO 6777–1984) for colorimetric nitrite identification. In general, raw materials or relevant functional groups are preserved on the CD surface during carbonization; such character has been extensively explored for constructing functional CDs with specifically discriminating or antimicrobial properties [26]. In view of this factor, we hypothesized that the preservation of NETH on CD surface is possible and the remained NETH may also support the Griess reaction. To understand whether the Griess reaction is feasible, chromogenic agent (*p*-aminobenzene sulfonic acid, SA) was introduced into NETH-CD solution in the presence of HCl and $NaNO_2$. It was observed that the NETH-CD solution color changed from light yellow to purple within 1 min (Fig. 3a inset), suggesting that azo compounds might form. Meanwhile, control experiments with only SA, HCl, or $NaNO_2$ were also conducted. As shown in Fig. 3a, simultaneous introduction of SA, HCl, and $NaNO_2$ into NETH-CD solution resulted in the appearance of new UV-visible absorption peak around 538 nm, which is assigned to the characteristic peak of azo dye. In contrast, the addition of $NaNO_2$ or mixtures (SA + HCl, SA + $NaNO_2$, or HCl + $NaNO_2$) didn't cause comparable variation to the UV-visible absorption spectra. The formation of azo dye also led to the fluorescence quenching of NETH-CDs. As

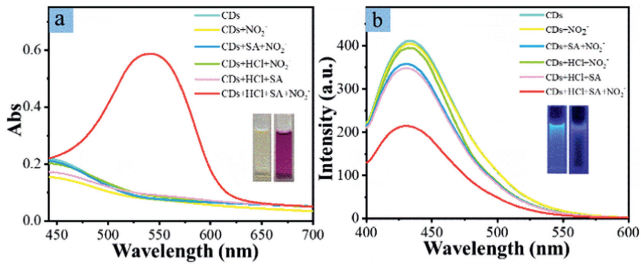


**Fig. 3.** Griess reaction-induced colorimetric and fluorometric variation of NETH-CD solution. UV–vis absorption (a) and fluorescence emission (b) spectra of NETH-CD solution without and with the addition of various species.

shown in Fig. 3b, the blue emission of NETH-CDs was dramatically suppressed upon adding SA, HCl, and $NaNO_2$. Similar to the colorimetric variation, addition of sole or two chemicals did not induce distinct fluorescence inhibition.

To verify the formation of azo dye, FT-IR and XPS characterization on NETH-CDs with the addition of $NaNO_2$ were performed. It was seen that the out of plane bending vibration of C-H on aromatic ring shifted from 937 $cm^{-1}$ to 974 $cm^{-1}$ upon adding $NaNO_2$ (Fig. S1 in Supporting information), indicating the formation of new chemical bonds. Meanwhile, a new peak around 1494 $cm^{-1}$ belongs to *N-N* stretch vibration was observed, revealing the formation of azo structure [27]. The binding of SA onto NETH-CDs was also proved by XPS spectra. The full XPS spectra of NETH-CDs with the addition of $NaNO_2$ showed enhanced C and N signals (Fig. S2a in Supporting information), implying the increased C and N contents NETH-CDs. The element ratio of C:N:O was calculated to be 7:1:11, which is higher than that of NETH-CDs. The C 1s spectrum was fitted with three components (Fig. S2b in Supporting information), including C–C/C=C (284.8 eV), C–OH (285.8 eV), and C–O/C–N (286.8 eV). The content ratio of three components was determined to be 0.7:1:3, which is lower than that of NETH-CDs (2:1:3). Accordingly, the N 1s spectrum was also fitted with three components (Fig. S2c in Supporting information), including N–H (399.7 eV), *N-N* (400.3 eV), and C–N (401.8 eV). The N-N content was calculated to be 47.5%, which further suggests the formation of azo dye. Therefore, both FT-IR and XPS characterizations demonstrate the feasibility of Griess reaction on NETH-CDs surface, which induces the colorimetric change and fluorescence quenching. The emission profile of NETH-CDs did not show visible change during Griess reaction, ruling out the inner filter effect. It should be noticed that the absorption spectra of resulted azo dye showed overlap with the emission spectra of NETH-CDs, which may result in the occurrence of inner filter effect or fluorescence resonance energy transfer. As the addition of nitrite, on profile changes in fluorescence emission spectra was observed, ruling out the occurrence of inner filter effect. Therefore, the occurrence of fluorescence resonance energy transfer is possible, accompanying with the decreased fluorescence lifetime of donor. To figure out this hypothesis, fluorescence lifetimes of NETH-CDs before and after Griess reaction were recorded. The fluorescence lifetime decreased from 17.19 ns to 4.18 ns after Griess reaction (Fig. S3 in Supporting information), suggesting the occurrence of fluorescence resonance energy transfer.

To investigate the reaction kinetics, time-dependent absorbance and fluorescence intensity variations of NETH-CD solution were monitored after adding of SA, HCl, and $NaNO_2$. As displayed in Fig. 4, the absorbance at 538 nm rapidly increased in a short time upon adding SA, and reached a flatform within 1 min. The relative fluorescence decrement also showed a rapid increase in 1 min reaction window. However, traditional Griess reaction with same concentrations of reactants showed complete reaction after 15 min.

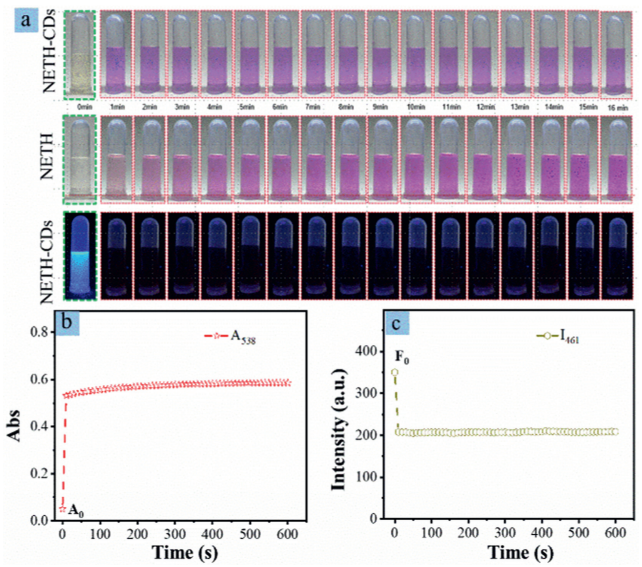


**Fig. 4.** Griess reaction kinetics on NETH-CD nanointerface. (a) Time-dependent photographs of NETH and NETH-CD solution upon adding nitrite under room light and UV light illumination. (b) Plots of the time-dependent 538 nm absorbance of NETH-CD solution upon adding nitrite. (c) Plots of the time-dependent 461 nm fluorescence intensity of NETH-CD solution upon adding nitrite.

The time-dependent absorbance of NETH for sensing nitrite was also investigated as a contrast (Fig. S4 in Supporting information). The absorbance gradually increased and reached the maximum at 15 min. This means the Griess reaction is distinctly accelerated on nanointerface. In partial recent works, fast reaction response were also found on CDs surface [28–30], and the accelerated reaction kinetics may benefit the exploration of CD-based sensitive detection systems.

The kinetics of chemical reactions is generally related to few parameters, including molecular collision probability and chemical reactivity [31–33]. The former is decided by molecular interaction and reactant concentration, while the latter dependents on the electronic distribution of reactants. In order to understand the mechanism of accelerated Griess reaction, Zeta potential measurements were first performed. As manifested in Fig. 5a, the surface charge of NETH in acidic condition was +24.2 mV, while the surface charge of NETH-CDs in same condition was −3.96 mV. In consideration of positively charged SA (+3.85 mV) in acidic condition, the negatively charged NETH-CDs can react with SA faster than NETH because of the electrostatic attraction [34,35]. The NETH-CDs not only diminish the electrostatic repulsion, but also facilitate the surface adsorption of SA due to the large specific area. The surface adsorption leads to the enrichment of reactants and increment of molecular collision probability, which accelerates the Griess reaction. In addition, the NETH concentration on NETH-CD surface was determined. After centrifugation of NETH-CDs solution, the generated azo dye in suspension decreased with the increasing NETH concentration, while it increased in NTEH-CDs collection (Fig. S5 in Supporting information), indicating high NETH concentration benifits its carbonization. According the UV–vis spectrometric measurement (Fig. 5b and Fig. S6 in Supporting information), about 3 to 5 NETH molecules existed on one NETH-CD. The localized and spatial NETH concentration was calculated to be 0.547 mol/L, which is much higher than that of free NETH in 0.015 mol/L solution. As a result, the enriched NETH on NETH-CD surface facilitates the occurrence of Griess reaction. After reaction, the formed surface azo compounds led to positive charge (Fig. 5c). In a word, the increased electrostatic attraction and localized NETH concentration, as well as the surface adsorption character, enhances the molecular colli-

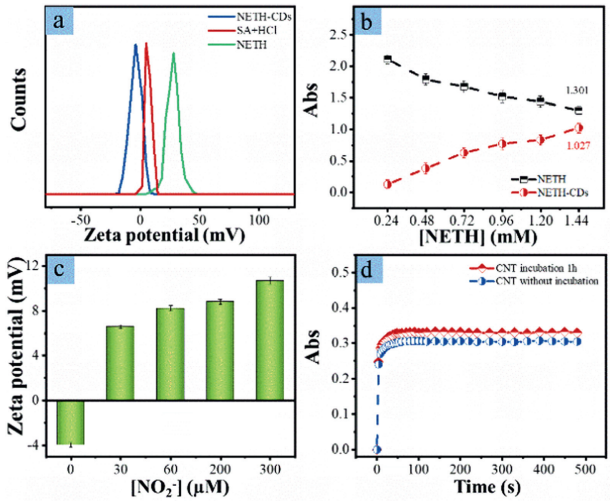


**Fig. 5.** Griess reaction kinetics on NETH-CD nanointerface. (a) Time-dependent photographs of NETH and NETH-CD solution upon adding nitrite under room light and UV light illumination. (b) Plots of the time-dependent 538 nm absorbance of NETH-CD solution upon adding nitrite. (c) Plots of the time-dependent 461 nm fluorescence intensity of NETH-CD solution upon adding nitrite. (d) Time-dependent 538 nm absorbance of NETH-CNT mixture in the presence of SA and HCl upon adding nitrite without and with 1 h incubation.

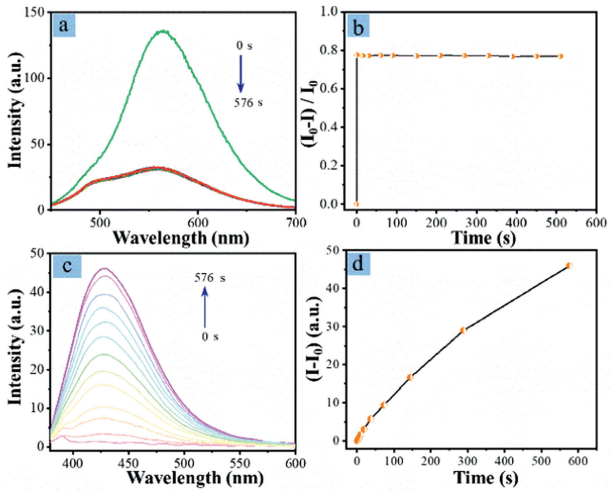


**Fig. 6.** Reaction kinetics of OPD-$Cu^{2+}$ system with and without carbonization treatment. Time-dependent fluorescence emission spectra of (a) E-CDs and (c) OPD solution with the addition of 5 μmol/L $Cu^{2+}$. The corresponding plots of fluorescence intensity *versus* reaction time were listed in (b) and (d).

sion probability, thus distinctly accelerates the Griess reaction on nanointerface.

It is reported that anion-$\pi$ interaction affects the electron-donating/withdrawing capability of the $\pi$-conjugation system, which changes its fluorescence and/or chemical reactivity [36]. Therefore, on the other hand, the electron-rich CD surface may interact with NETH and enhance its corresponding nucleophilicity. To demonstrate this assumption, nucleophilicity regulation of NETH by another electron-rich carbon material, carbon nanotube (CNT) was conducted. After surface adsorption, the kinetics of Griess reaction was enhanced on CNT surface, as displayed in Fig. 5d. Further incubation did not cause visible increment of reaction kinetics, indicating the electron-$\pi$ interaction is rapid. Notice that the reaction kinetics of CNT-NETH mixture was slower than that with NETH-CDs, the enhanced nucleophilicity is not the only reason for the boosted reaction kinetics. Thus, the carbonization enhanced electrostatic attraction, reactant concentration and nucleophilicity, diminish the reaction energy barrier and promote the Griess reaction. Taken together, carbonization-engineered ultrafast nanointerfacial Griess reaction is attributed the synergic action of reduced electrostatic repulsion, enriched reactant concentration and boosted NETH nucleophilicity. We also tried to prepara CDs with SA as the raw materials, which may further support the accelerated nanointerfacial reaction. However, no fluorescence of SA solution after electrolysis treatment was observed (Fig. S7 in Supporting information), suggesting the unsuccessful carbonization of SA. This might be atributed to A possible reason for this phenomenon is that the strongly negative charge of sulfonic acid group hinders the approaching of SA monomer, which limits the dehydration, polymerization, and subsequent carbonization. Similar results also appeared in citric acid cases, and additives were usually required to produce CDs [23,24].

To verify the universality of the carbonization-engineered ultrafast chemical reaction strategy, OPD was carbonized by both electrochemical method and hydrothermal treatment (denoted as E-CDs and H-CDs) for sensing AA and $Cu^{2+}$, respectively. The FT-IR and HRTEM images demonsted the production of E-CDs and H-CDs (Figs. S8 and S9 in Supporting information). The E-CDs showed excitation and emission maxima at 418 and 565 nm (Fig. S10 in Supporting information), respectively. However, the H-CDs showed only ultraweak emission due to the absence of surface 2,3-diaminophenazine. OPD can react with AA under alkyline condition and form quinoxaline [37], which has strong absorbance at 340 nm and blue fluorescence at 427 nm (Fig. S11 in Supporting information). The blue emission from OPD and AA mixture gradually increased even after 576 s reaction (Fig. 6). Using E-CDs as the reactants, the fluorescnece at 575 nm was immediately quenched in 20 s after adding AA. The quenched fluorescence is probably due to the photon-induced electron transfer between quinoxaline and E-CDs. This means the carbonization strategy is appliable to accelerate the raction kinetics of OPD-AA system. In addition, the $Cu^{2+}$-catalytic oxidation of OPD forms yellow-emissive 2,3-diaminophenazine product. The H-CDs showed no fluorescence, and the yellow emission gradually increased after the addition of 5 μmol/L $Cu^{2+}$. The fluorescence intensity around 572 nm reached a flatform after 35 min reaction (Fig. S12 in Supporting information). In constrast, the emission of OPD-$Cu^{2+}$ solution at 560 nm remained increment even after 105 min (Fig. S13 in Supporting information), suggesting the rapid reaction rate after carbonization. The enhanced reaction rate in both OPD-AA and OPD-$Cu^{2+}$ systems validate that the proposed carbonization-enhanced reaction kinetics strategy is applicable in diverse systems. In addition, the $Cu^{2+}$ had no effect on the fluorescence emission spectrum of E-CDs (Fig. S14 in Supporting information), indicating the surface chemical bond-related fluorescence and recognition behaviors [38]. In this case, some limitations of such a carbonization-engineered ultrafast nanointerfacial chemical reaction may exist. In our opinon, three parameters are important. (1) The organic raw materials can be readily converted into CDs. (2) The preservation of functional groups during the carbonization treatment. (3) Electrostatic attraction shows influence on the reaction kinetics. Therefore, the carbonization accelerated chemical reaction may not be universally applicable for all reaction systems. Still, we believe the increment of reaction kinetics might improve the sensitivity in further analytical applications.

In summary, we discover that the Griess reaction kinetics can be greatly improved by changing molecular reactant (NETH) into fluorescent CDs *via* carbonization strategy. The carbonization makes NETH-CDs more reactive to SA in acidic environment. The accelerated Griess reaction is attributed the synergic action of carbonization-enhanced electrostatic attraction, enriched localized and spatial NETH concentration, and boosted NETH nucleophilicity. And such a promotion does not change the reaction speci-

ficity in comparison to conventional Griess assay. The fluorometric and colorimetric variations endow NETH-CDs excellent candidates for achieving ultrafast and dual-channel nitrite sensing. In addition, the boosted reaction kinetics in OPD-AA and OPD-$Cu^{2+}$ systems verify the universality of carbonization-engineered ultrafast chemical reaction on nanointerface. Ultrafast chemical reactions possess potentials in chemical/biological processes monitoring, active intermediate identification, and dynamic variation recording; this work illuminates that the nanointerface chemistry can significantly promote the chemical reaction kinetics. We identify that the incorporation of nanointerfacial chemistry into the ultrasmall nanoparticles may provide new horizons in developing multifunctional nanomaterials to realize ultrafast analysis in biological, material, and industrial aspects. Therefore, we believe our work will be generally useful for biologists, chemists, nanotechnologists, as well as engineers for developing next-generation nanoparticles as effective nanoreactants and reporters.

## Declaration of competing interest

The authors declare that they have no known competing financial interests or personal relationships that could have appeared to influence the work reported in this paper.

## Acknowledgments

This work was supported by the National Natural Science Foundation of China (Nos. 82160153, 21505162, 22074005, and 22101027), Natural Science Foundation of Hunan Province, China (No. 2022SK2102), Hunan Provincial Department of Education Scientific Research Project (No. 240994), and the Natural Science Foundation of Beijing Municipality (No. 2202038). Z. Yuan thanks Mrs. Yu Kang at Analysis and Test Center of Beijing University of Chemical Technology for the assistance of quantum yield and lifetime measurements.

## Supplementary materials

Supplementary material associated with this article can be found, in the online version, at doi:10.1016/j.cclet.2024.109728.

## References

[1] Y. Fu, N.A. Simeth, R. Toyoda, et al., Angew. Chem. Int. Ed. 62 (2023) e202218203.
[2] M.F. Nüesch, M.T. Ivanović, J.B. Claude, et al., J. Am. Chem. Soc. 144 (2022) 52–56.
[3] T. Patriarchi, J.R. Cho, K. Merten, et al., Science 360 (2018) eaat4422.
[4] F. Li, X. Mao, F. Li, et al., J. Am. Chem. Soc. 142 (2020) 9975–9981.
[5] Y. Liu, X. Du, Z. Wang, et al., J. Colloid Interface Sci. 609 (2022) 289–296.
[6] O.A. Sytina, D.J. Heyes, C.N. Hunter, et al., Nature 456 (2008) 1001–1004.
[7] C.F. Chang, H. Kuramochi, M. Singh, et al., Angew. Chem. Int. Ed. 61 (2022) e202111930.
[8] M. Xu, D. Li, K. Sun, et al., Angew. Chem. Int. Ed. 60 (2021) 16372–16376.
[9] S. Narayan, J. Muldoon, M.G. Finn, et al., Angew. Chem. Int. Ed. 44 (2005) 3275–3279.
[10] M.F. Ruiz-Lopez, J.S. Francisco, M.T.C. Martins-Costa, J.M. Anglada, Nat. Rev. Chem. 4 (2020) 459–475.
[11] J. Zhang, L. Mou, X. Jiang, Chem. Sci. 11 (2020) 923–936.
[12] H. Liu, P. Tan, Y. Liu, et al., J. Colloid Interface Sci. 619 (2022) 246–256.
[13] R. Buonsanti, D.J. Milliron, Chem. Mater. 25 (2013) 1305–1317.
[14] T. Yuan, F. Yuan, L. Sui, et al., Angew. Chem. Int. Ed. 62 (2023) e202218568.
[15] S. Mondal, S.R. Das, L. Sahoo, S. Dutta, U.K. Gautam, J. Am. Chem. Soc. 144 (2022) 2580–2589.
[16] D.C. Green, M.A. Holden, M.A. Levenstein, et al., Nat. Commun. 10 (2019) 206.
[17] Q. Ye, T. Dai, J. Shen, et al., J. Anal. Test. 7 (2023) 16–24.
[18] T.T. Zhang, Z.H. Chen, G.Y. Shi, M. Zhang, J. Anal. Test. 6 (2022) 365–373.
[19] Q. An, Q. Lin, X. Huang, et al., Dyes Pigm. 185 (2021) 108878.
[20] D. Xu, Y. Huang, Q. Ma, et al., Chem. Eng. J. 456 (2023) 141104.
[21] R. Atchudan, T.N.J.I. Edison, S. Mani, et al., Dalton Trans. 49 (2020) 17725–17736.
[22] X. Yang, Y. Zhuo, S. Zhu, et al., Biosens. Bioelectron. 60 (2014) 292–298.
[23] J. Schneider, C.J. Reckmeier, Y. Xiong, et al., J. Phys. Chem. C 121 (2017) 2014–2022.
[24] H. Yang, F. Lu, X. Zhan, et al., Talanta 208 (2020) 120368.
[25] D. Li, Y. Ma, H. Duan, W. Deng, D. Li, Biosens. Bioelectron. 99 (2018) 389–398.
[26] H.W. Chu, B. Unnikrishnan, A. Anand, Y.W. Lin, C.C. Huang, J. Food Drug Anal. 28 (2020) 539–557.
[27] H. Wu, X. Shen, D. Huo, et al., Spectrochim. Acta Part A 225 (2020) 117470.
[28] Y. Jia, Z. Cheng, G. Wang, et al., Food Chem. 402 (2023) 134245.
[29] X. Zhu, X. Yuan, L. Han, H. Liu, B. Sun, Biosens. Bioelectron. 191 (2021) 113460.
[30] F. Hu, Q. Fu, Y. Li, et al., Food Chem. 431 (2024) 137097.
[31] D.K. Hoffmann, T. Paintner, W. Limmer, D.S. Petrov, J.H. Denschlag, Nat. Commun. 9 (2018) 5244.
[32] A. Kreft, A. Lücht, J. Grunenberg, P.G. Jones, D.B. Werz, Angew. Chem. Int. Ed. 58 (2019) 1955–1959.
[33] G. Graziano, Nat. Rev. Chem. 2 (2018) 0127.
[34] Y. Yu, Z. Yuan, C. Lu, Aggregate 4 (2023) e349.
[35] M. Jin, L. Huang, Y. Tang, et al., Sens. Actuator. B 297 (2019) 126748.
[36] N. Luo, Y.F. Ao, D.X. Wang, Q.Q. Wang, Angew. Chem. Int. Ed. 60 (2021) 20650–20655.
[37] D. Zhao, J. Li, C. Peng, et al., Anal. Chem. 91 (2019) 2978–2984.
[38] F. Shan, J. Zhang, C. Liao, Z. Wang, L. Wang, Chin. Chem. Lett. 34 (2023) 108107.